

Localization on a Synthetic Hall Cylinder

Ren Zhang^{1,2}, Yangqian Yan², and Qi Zhou²

¹*School of Physics, Xi'an Jiaotong University, Xi'an, Shaanxi 710049, China*

²*Department of Physics and Astronomy, Purdue University, West Lafayette, Indiana 47907, USA*



(Received 10 December 2020; accepted 20 April 2021; published 10 May 2021)

By engineering laser-atom interactions, both Hall ribbons and Hall cylinders as fundamental theoretical tools in condensed matter physics have recently been synthesized in laboratories. Here, we show that turning a synthetic Hall ribbon into a synthetic Hall cylinder could naturally lead to localization. Unlike a Hall ribbon, a Hall cylinder hosts an intrinsic lattice, which arises due to the periodic boundary condition in the azimuthal direction, in addition to the external periodic potential imposed by extra lasers. When these two lattices are incommensurate, localization may occur on a synthetic Hall cylinder. Near the localization-delocalization transitions, physical observables strongly depend on the axial magnetic flux, providing us a sensitive means to probe either the transition or the axial flux using one another. In the irrational limit, physical observables are no longer affected by the axial flux, signifying a scheme to suppress decoherence induced by fluctuations of the axial flux.

DOI: [10.1103/PhysRevLett.126.193001](https://doi.org/10.1103/PhysRevLett.126.193001)

Lasers could change the momentum of an atom and meanwhile flip its spin, laying the foundation of synthetic spin-orbit coupling for charge-neutral atoms [1–12]. Viewing spins as a synthetic dimension [13,14], a one-dimensional spin-orbit coupled system is equivalent to a two-dimensional quantum Hall ribbon [15,16]. Synthetic dimensions also allow physicists to access high-dimensional physics [17], such as a four-dimensional charge pump [18,19]. Another profound advantage is the controllable boundary condition [20]. Several groups have recently realized synthetic Hall cylinders by implementing periodic boundary conditions in the synthetic dimensions [21–23]. In such a synthetic Hall cylinder, in addition to a uniform axial synthetic magnetic flux ϕ , an extra magnetic flux Φ can be created at one end surface. Consequently, the total magnetic flux through the cylindrical surface becomes finite, a challenging task for a cylinder in real space such as a nanotube.

Two different scenarios have been used in synthetic Hall ribbons and synthetic Hall cylinders. In experiments done at Florence, NIST, and Seoul [15,16,21], extra lasers impose external optical lattices in the real dimensions. Hamiltonians are constructed based on these external optical lattices. However, in the experiment done at Purdue [22] and another one at NIST [23], no external lattice is applied. The density modulation developed on the Hall cylinder purely comes from the periodic boundary condition in the synthetic dimension. This is referred to as the intrinsic lattice of the Hall cylinder. Fundamental questions arise of whether the interplay between the intrinsic and the external lattice leads to any qualitatively new physics, and whether the Hall ribbon and the Hall cylinder could host distinct quantum phenomena.

The main results of this Letter are summarized as follows. (I) Localization could occur on a Hall cylinder when the external lattice is incommensurate with the intrinsic one. (II) The intrinsic lattice is absent in a Hall ribbon, and hence the localization on the Hall cylinder disappears, reflecting the significance of the boundary conditions in synthetic spaces. (III) For any commensurate lattices, the dependence of physical observables, for instance, the inverse participation ratio, on ϕ is maximized near the delocalization to localization transitions. This delivers a sensitive scheme to measure either the transition or ϕ using one another. In the irrational limit, the dependence becomes weaker and eventually vanishes, signifying a unique means to suppress the decoherence induced by fluctuating ϕ . (IV) For a Bose-Einstein condensate in the Hall cylinder, the delocalization-localization transition is robust to the weak interaction. (V) It is well known that any irrational number can be approximated by a rational number to arbitrary precision. This fact manifests itself in our system such that the localization is observable in a finite Hall cylinder with commensurate lattices.

Hamiltonian and eigenstates.—The synthetic dimension can be encoded in internal states, either hyperfine spins of alkali-metal atoms [16,21–23] or nuclear spins of alkaline-earth metal atoms [15]. We consider N sites (N internal states) in the synthetic dimension. As shown in Fig. 1(a), the intersite hopping is accomplished by Raman lasers or microwave fields flipping hyperfine or nuclear spins. In the real dimension, extra counterpropagating lasers impose an external one-dimensional optical lattice, the lattice spacing of which is π/k_L . k_L is the wave number of the extra lasers. The Hamiltonian is written as

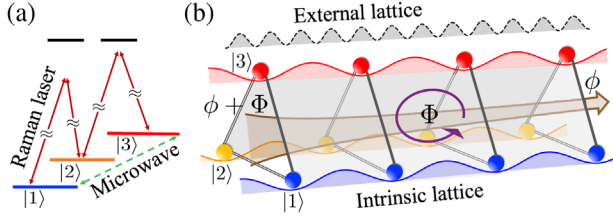


FIG. 1. A schematic of a synthetic Hall cylinder formed by three internal states. (a) The same Raman lasers couple $|\psi_1(x)\rangle$ and $|\psi_2(x)\rangle$, $|\psi_2(x)\rangle$, and $|\psi_3(x)\rangle$. The coupling between $|\psi_3(x)\rangle$ and $|\psi_1(x)\rangle$ is provided by a two-photon microwave transition. (b) In the real dimension, an external optical lattice is imposed, in addition to the intrinsic lattice on a Hall cylinder. The synthetic flux at the two ends of the Hall cylinder are ϕ and $\phi + \Phi$, respectively, where Φ is equal to the flux penetrating the cylindrical surface.

$$\hat{H}_0 = \sum_{j=1}^N |\psi_j(x)\rangle \left[-\frac{\hbar^2}{2M} \partial_x^2 + V \sin^2(k_L x) + \epsilon_j \right] \langle \psi_j(x) | + \sum_{j=1}^N \frac{\Omega_j}{2} e^{2ik_j x + i\phi_j} |\psi_{j+1}(x)\rangle \langle \psi_j(x) | + \text{H.c.}, \quad (1)$$

where $|\psi_j(x)\rangle$ is the j th internal state with spatial wave function $\psi_j(x)$, V the depth of the optical lattice, and ϵ_j the detuning in the Raman or microwave transition. Ω_j denotes the coupling strength between internal state j and $j+1$ induced by the Raman lasers or a microwave with a wave number k_j and phase ϕ_j , and $\psi_{N+1}(x) = \psi_1(x)$. $k_j = 0$ if it is induced by the microwave.

Along a closed-loop, $(x_0, j) \rightarrow (x_0, j+1) \rightarrow (x_0 - \Delta x, j+1) \rightarrow (x_0 - \Delta x, j) \rightarrow (x_0, j)$, an atom accumulates an extra phase $2k_j \Delta x$, where Δx denotes the distance along the real dimension. The total magnetic flux penetrating the cylindrical surface, $\Phi = \sum_j 2k_j L$, where L is the length of the cylinder, originates from the nonuniform axial flux that can be used to access topological charge pumping [24]. As shown in Fig. 1(b), the axial flux includes a uniform part ϕ and a gradient that leads to different flux through the two ends, ϕ and $\phi + \Phi$, respectively. The periodic boundary condition (PBC) and open boundary condition (OBC) corresponds to $\Omega_N \neq 0$ and $\Omega_N = 0$, respectively. Ω_N is the coupling between the first internal state and the N th one. For PBC or OBC, we refer to this system as a synthetic Hall cylinder or synthetic Hall ribbon, respectively. On the Hall cylinder, H_0 gives rise to an intrinsic periodic lattice even when $V = 0$ [25].

Hereafter, we consider a minimum Hall cylinder ($N = 3$). Furthermore, we consider that the coupling between $|\psi_1(x)\rangle$ and $|\psi_2(x)\rangle$ is provided by the same Raman lasers that couple $|\psi_2(x)\rangle$ and $|\psi_3(x)\rangle$. $|\psi_3(x)\rangle$ and $|\psi_1(x)\rangle$ are coupled by a two-photon microwave transition, the strength of which is taken equal to the Raman couplings. As a result, in such a configuration

$k_1 = k_2 = k_0$, $k_3 = 0$, and $\Omega_{j=1,2,3} = \Omega$. In practice, this configuration can be realized in current experiments [21,22]. Each single ϕ_j can be gauged away but the sum of all phases, $\phi = \sum_j \phi_j$, is an important quantity to control system. For convenience, we set $\phi_1 = \phi_2 = 0$, $\phi_3 = \phi$. Since finite detunings ϵ_j typically exist and the synthetic magnetic flux may also be nonuniform in experiments, the ground state of our system is unique.

The periodicity of the density modulation in the intrinsic lattice is $d_I = \pi/(2k_0)$, and the lattice spacing of the external optical lattice is $d_E = \pi/k_L$. We use d_T to denote the lattice spacing of the composite lattice that consists of the intrinsic and external lattices. d_T is the least common multiple (LCM) of d_I and d_E ,

$$d_T = f_{\text{LCM}}(d_I, d_E). \quad (2)$$

We consider a sequence of commensurate lattices that satisfy

$$\left(\frac{d_I}{d_E} \right)_l = \left(\frac{k_L}{2k_0} \right)_l = \frac{f_{l+1}}{2f_l}, \quad (3)$$

where $f_l = \{1, 1, 2, 3, 5, 8, \dots\}$ is the Fibonacci sequence with $l = 1, 2, 3, \dots$. It is known that $\lim_{l \rightarrow \infty} f_{l+1}/f_l = (\sqrt{5} + 1)/2$, i.e., in the large l limit, a rational number, f_{l+1}/f_l , well approximates the golden ratio.

Figure 2 shows how \hat{H}_0 couples a sequence of plane waves, $|q_j + 4mk_0 + 2nk_L\rangle_j$, where m and n are integers and $q_j = q + 2(j-1)k_0$. A plane wave of the j th spin state $|q_j\rangle_j$ has an on-site energy of $\epsilon_j + \hbar^2 q_j^2/(2M)$. The intersite couplings of this momentum space lattice are provided by Raman couplings, microwave transitions, and the external lattice, as specified in Fig. 2. An eigenstate is written as

$$|\Psi(q)\rangle = \sum_{j,m,n} c_{j,m,n} |q_j + 4mk_0 + 2nk_L\rangle_j. \quad (4)$$

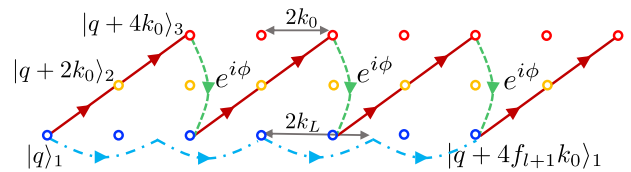


FIG. 2. Illustration of coupling pathways in the momentum space. One pathway is provided by the Raman (red solid arrow) and microwave (green dashed) transitions, which transfers momentum $4k_0$ and accumulate a phase ϕ . Another pathway is provided by the external lattice (blue dash-dotted) which transfers momentum $2k_L$. After f_{l+1} times Raman and microwave transition or $2f_l$ times external lattice coupling, the two pathways meet. Here, we take $l = 3$ as an example.

When $2k_0/k_L$ or equivalently, d_E/d_I , is commensurate, two plane waves are coupled by multiple pathways. For instance, Fig. 2 shows two pathways coupling $|q\rangle_1$ and $|q + 4f_{l+1}k_0\rangle_1$, one given by the intrinsic lattice and the other by the external lattice. As shown later, the interference between such pathways becomes crucial when discussing the delocalization to localization transition. The detuning ϵ_j means an energy barrier for particles to tunnel in the synthetic dimension. If the detuning is large, it will be difficult for particles to move along the trajectory shown by the red and green arrows in Fig. 2. Thus, the Raman couplings and microwave couplings need to be large enough to overcome the energy barrier to induce the localization-delocalization transition.

Delocalization to localization transition.—Localization is often studied using the Aubry-André model, which considers particles subject to a random potential [26]. In ultracold atoms, a quasiperiodic lattice was realized by imposing two incommensurate optical lattices to mimic the randomness [27–29], and the delocalization to localization transition has been observed in bosons [30,31]. Here, we show that the delocalization to localization transition naturally emerges on a Hall cylinder. Two conditions are required for the localization on a Hall cylinder. (i) The intrinsic and the external lattice are incommensurate, which leads to a random potential for the bosons. (ii) The potential energy dominates over the kinetic energy, i.e., the amplitude of the composite potential should be large enough to suppress the motion along the real dimension.

We consider a prototypical irrational number, $k_L/k_0 = (\sqrt{5} + 1)/2$, which can be approximated by the ratio of two rational numbers, i.e., the aforementioned f_{l+1}/f_l , Fibonacci sequence. In the large l limit, results of incommensurate lattices can be well approximated by commensurate lattices in a finite system. Strictly speaking, localization exists only for incommensurate lattices, i.e., when $l \rightarrow \infty$. For any finite l , $(k_L/k_0)_l = f_{l+1}/f_l$, the external and intrinsic lattices are commensurate. However, when l is large enough, a length scale separation exits, $\sigma \ll L \ll d_T$, where σ is the width of the wave function in a unit cell of the composite lattice and L is the system size. Experiments conducted on such a finite system will well reproduce physics observables in an incommensurate lattice, such as the density distribution.

To quantify the localization, we consider the dimensionless inverse participation ratio (IPR) [32],

$$\alpha_{\text{IPR}} = \frac{\int_0^{d_T} dx [\sum_{j=1}^3 |\psi_j(x)|^2]^2}{k_0 [\int_0^{d_T} dx \sum_{j=1}^3 |\psi_j(x)|^2]^2}. \quad (5)$$

For convenience, we have used the total density of all three spin states to compute IPR. In the ideal delocalized states, i.e., $|\psi_j(x)|^2$ is uniform, $\text{IPR} \propto 1/d_T$, which approaches

zero in the large l limit. In the ideal localized states, i.e., $|\psi_j(x)|^2 = \delta(x)$, IPR diverges. In a finite system, IPR remains small in the delocalized state. Tuning V and Ω , the state becomes localized and IPR quickly increases to a large value.

A density plot of IPR as a function of Ω and V is illustrated in Fig. 3(a). It is obvious that when either Ω or V is fixed and the other increases, IPR increases. For instance, when $\Omega = 2E_0$ and $V = 5E_0$, as shown by the red circle, $\text{IPR} \sim 0.1$, and the density distribution is shown in Fig. 3(b). The Raman laser recoil energy $E_0 = \hbar^2 k_0^2 / 2m$ is used as the energy unit throughout. It is clear that the density distribution extends to the whole unit cell of the composite lattice. In contrast, when $\Omega = 8E_0$ and $V = 18E_0$, as shown by the red rectangle, IPR is around the unit, and the density distribution is shown in Fig. 3(c). The density distribution now is spatially localized in each unit cell, i.e., $\sigma \ll d_T$. More interestingly, there is a clear boundary between the delocalized regime and the localized regime on the density plot of IPR. Near the boundary, IPR increases very quickly from a small value to a large one, which implies the transition from the delocalized state to the localized state. In our calculation, we take $l = 9$ meaning $k_L/k_0 = 55/34$. Thus, the composite lattice is readily a good approximation for an incommensurate lattice in a finite system, the size of which satisfies $\sigma \ll L \ll d_T$. It is reasonable to expect that with increasing l such that $k_L/k_0 \rightarrow (\sqrt{5} + 1)/2$, the transition becomes even sharper,

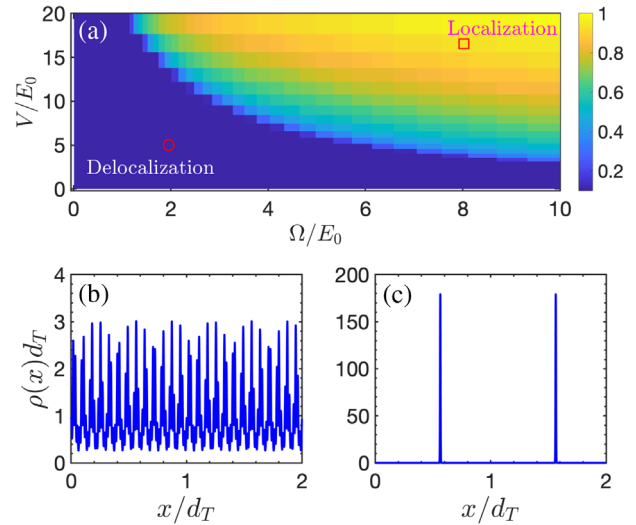


FIG. 3. (a) Inverse participation ratio (IPR) of the synthetic Hall cylinder. The color bar denotes the density of the dimensionless IPR. (b) A typical ground state density distribution $\rho(x) = \sum_{j=1}^3 |\psi_j(x)|^2$ in the delocalized regime (red circle), where $\Omega = 2E_0$, $V = 5E_0$ with $E_0 = \hbar^2 k_0^2 / 2m$ being the Raman laser recoil energy. (c) A typical ground state density distribution in the localized regime (red rectangle), where $\Omega = 8E_0$, $V = 18E_0$. The density distribution in two unit cells is shown. In our calculation, $\epsilon_1 = -0.1E_0$, $\epsilon_2 = 0$, $\epsilon_3 = 0.1E_0$, $\phi = \pi/3$, and $l = 9$.

which serves as a smoking gun of the delocalization to localization transition.

We would like to point out that PBC is crucial. Under OBC, the intrinsic lattice vanishes. Without the external lattice, the density becomes uniform in the real dimension. Turning on a finite V , though the density becomes periodically modulated, because of the absence of intrinsic lattice, the delocalization to localization transition on a Hall cylinder disappears. For more properties regarding the delocalization-localization transition, please refer to Supplemental Material (SM) [33].

Dependence on the uniform axial synthetic flux.—According to Eq. (1), the wave function accumulates a constant phase factor ϕ after a closed-loop motion $|\psi_1(x)\rangle \rightarrow |\psi_2(x)\rangle \rightarrow |\psi_3(x)\rangle \rightarrow |\psi_1(x)\rangle$. In practice, the phases of the Raman lasers are in general different from those of the microwaves. ϕ is thus finite and tunable. This corresponds to the uniform part of the axial flux and determines the origin of the intrinsic lattice. In the absence of the external lattice, physical observables in an infinite system do not depend on ϕ because of the translational invariance. However, when the external lattice is turned on, ϕ cannot be ignored as it determines the relative displacement between the intrinsic and external lattices. Alternatively, one could consider the Hamiltonian in the momentum space, as shown in Fig. 2. When k_L/k_0 is a rational number, e.g., f_{l+1}/f_l , multiple pathways contribute to the occupancy in a single plane wave. The uniform flux ϕ , which determines the relative phase between different pathways, becomes crucial, in particular near the delocalization to localization transition. This allows one to quantitatively trace how good the rational approximation of an irrational number is.

To this end, we calculate the dependence of IPR on ϕ . Our results indicate that for any commensurate lattice, i.e., a finite l , IPR depends on ϕ , as expected. However, in both the delocalized state and the localized state, such dependence is weak, as either the intrinsic or the external lattice is much stronger than the other one. Shifting their relative position by changing ϕ does not lead to considerable changes in IPR, as shown in Fig. 4. In contrast, the dependence is maximized near the transition point, where the amplitudes of these two lattices become comparable. Changing the relative displacement thus significantly changes the property of the system. For the variance of IPR, please refer to SM 5.

It is worth pointing out that our results are particularly useful in practice, when ϕ may fluctuate in repeated experiments [24]. Our findings indicate that near the delocalization to localization transitions, fluctuations in ϕ may lead to a large variance of physical observables. If we examine IPR more carefully near the transition point, its periodic dependence on ϕ is shown in Figs. 4(a) and 4(c). Interestingly, such periodicity directly unfolds l we used in the Fibonacci sequence. Consider a change in ϕ ,

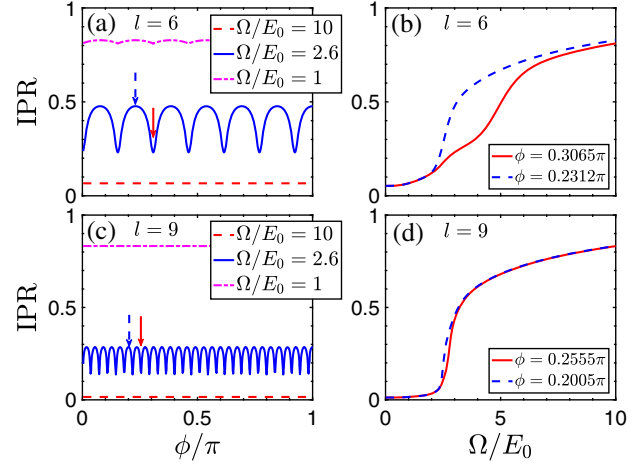


FIG. 4. (a),(c) Dependence of IPR on the constant part of the axial synthetic flux ϕ for two rational approximations. f_{l+1} counts the oscillations. (b),(d) IPR as a function of Raman coupling strength for given external lattice and flux. The values of ϕ are indicated by the arrows in (a) and (c). In our calculation, $V = 10E_0$, $\epsilon_1 = -0.1E_0$, $\epsilon_2 = 0$, $\epsilon_3 = 0.1E_0$.

$\phi \rightarrow \phi + \Delta\phi$. $\Delta\phi$ can be gauged away by multiplying $|q_j + 4mk_0 + 2nk_L\rangle_j$ an extra phase $e^{im\Delta\phi}$. Thus, $|q_j + 4f_{l+1}k_0\rangle_j$, or equivalently, $|q_j + 4f_l k_L\rangle_j$, acquires additional phase, $e^{if_{l+1}\Delta\phi}$, after the transformation. Meanwhile, $|q_j + 4f_{l+1}k_0\rangle_j$ are coupled to $|q_j\rangle_j$ by the external lattice potential, resulting in the same additional phase $e^{if_{l+1}\Delta\phi}$ acquired by $|q_j\rangle_j$. To ensure the single valuedness of the wave function, $e^{if_{l+1}\Delta\phi} = 1$ has to be satisfied. The periodicity of a physical observable, such as IPR, as a function of ϕ , is given by $2\pi/f_{l+1}$. We thus conclude that measuring the dependence of IPR or other physical observables on ϕ directly allows us to quantitatively trace the precision of using rational numbers to approximate an irrational number.

Another notable result arises when increasing the precision of the rational approximation of $(\sqrt{5} + 1)/2$. With increasing l , the dependence of IPR on ϕ weakens and eventually vanishes in the incommensurate lattice. For $l = 9$, the dependence is less obvious than that of $l = 6$, as shown in Figs. 4(b) and 4(d). Increasing l means enlarging the length of the pathways that interfere with each other in Fig. 2. Since $|q_j + 4f_{l+1}k_0\rangle_j$ has a larger on-site energy than $|q_j\rangle_j$, larger f_{l+1} correspond to a weaker coupling between these two states. As a result, the relative phase of these two pathways becomes less important. In particular, in the limit $l \rightarrow \infty$, these two pathways will never meet, as the incommensurate intrinsic and external lattices could not couple $|q_j\rangle_j$ to the same plane wave at all. We thus conclude that the dependence vanishes in the incommensurate lattice. This phenomenon has been observed in a recent experiment at NIST [36]. Our incommensurate lattice corresponds to the irrational

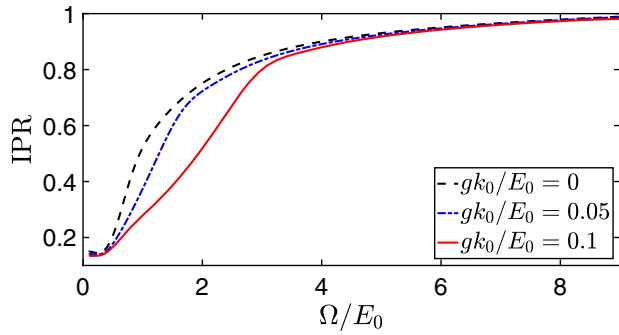


FIG. 5. Interaction effect on IPR. In our calculation, $V = 20E_0$, $\hbar\omega = 0.05E_0$, $\epsilon_1 = -0.1E_0$, $\epsilon_2 = 0$, $\epsilon_3 = 0.1E_0$, $l = 7$.

transverse flux that suppresses decoherence caused by fluctuations in the axial flux in the experiment.

Interaction effects.—In realistic experiments, weak interactions exist in a Bose-Einstein condensate uploaded to a synthetic Hall cylinder [5](#). For simplicity, we consider a quasi-1D system in the real dimension and equal and repulsive interspin and intraspin interactions, $U = (g/2) \int dx \rho(x)^2$ where $\rho(x) = \sum_{j=1}^3 \psi_j^\dagger(x) \psi_j(x)$ denotes the atomic density, g the interaction strength. We include the harmonic trap in the real dimension. By numerically solving the imaginary-time Gross-Pitaevskii equation,

$$-\frac{\partial \vec{\psi}(x)}{\partial \tau} = \left(\hat{H}_0 + \frac{1}{2} M \omega^2 x^2 + g \rho(x) \right) \vec{\psi}(x), \quad (6)$$

with $\vec{\psi}(x) = [\psi_1(x), \psi_2(x), \psi_3(x)]$ and ω the trapping frequency, we obtain the ground state and hence the IPR. In [Fig. 5](#), we show the IPR for various interaction strength. Our results show the weak repulsive interaction in current experiments slightly changes the IPR but the qualitative features of the noninteracting systems remain.

In summary, we have studied the delocalization to localization transition on a Hall cylinder due to the interplay between the intrinsic lattice and the external lattice. Our results provide experimentalists with a unique platform to study new quantum phenomena and to address fundamental questions in synthetic spaces. We hope that our work will stimulate the community to explore more synthetic spaces.

Q.Z. acknowledges a useful conversation with Ian Spielman at Sant Feliu that inspired us to expand discussions on the constant part of the axial flux. We are also grateful to Ian Spielman and Qi-Yu Liang to share their manuscript prior to submission. R.Z. is supported by the National Key R&D Program of China (Grant No. 2018YFA0307601), NSFC (Grant No. 11804268). Q.Z. and Y.Y. are supported by National Science Foundation (NSF) through Grant No. PHY-1806796, the Air Force Office of Scientific Research under Grant No. FA9550-20-1-0221, and a seed fund from Purdue Quantum Science and Engineering Institute.

- [1] Y. J. Lin, R. L. Compton, K. Jiménez-García, J. V. Porto, and I. B. Spielman, Synthetic magnetic fields for ultracold neutral atoms, *Nature (London)* **462**, 628 (2009).
- [2] Y. J. Lin, K. Jiménez-García, and I. B. Spielman, Spin-orbit-coupled Bose-Einstein condensates, *Nature (London)* **471**, 83 (2011).
- [3] P. Wang, Z.-Q. Yu, Z. Fu, J. Miao, L. Huang, S. Chai, H. Zhai, and J. Zhang, Spin-Orbit Coupled Degenerate Fermi Gases, *Phys. Rev. Lett.* **109**, 095301 (2012).
- [4] L. W. Cheuk, A. T. Sommer, Z. Hadzibabic, T. Yefsah, W. S. Bakr, and M. W. Zwierlein, Spin-Injection Spectroscopy of a Spin-Orbit Coupled Fermi Gas, *Phys. Rev. Lett.* **109**, 095302 (2012).
- [5] L. F. Livi, G. Cappellini, M. Diem, L. Franchi, C. Clivati, M. Frittelli, F. Levi, D. Calonico, J. Catani, M. Inguscio, and L. Fallani, Synthetic Dimensions and Spin-Orbit Coupling with an Optical Clock Transition, *Phys. Rev. Lett.* **117**, 220401 (2016).
- [6] S. Kolkowitz, S. L. Bromley, T. Bothwell, M. L. Wall, G. E. Marti, A. P. Koller, X. Zhang, A. M. Rey, and J. Ye, Spin-orbit-coupled fermions in an optical lattice clock, *Nature (London)* **542**, 66 (2017).
- [7] B. Song, C. He, S. Zhang, E. Hājijev, W. Huang, X.-J. Liu, and G.-B. Jo, Spin-orbit-coupled two-electron Fermi gases of ytterbium atoms, *Phys. Rev. A* **94**, 061604(R) (2016).
- [8] V. Galitski and I. B. Spielman, Spin-orbit coupling in quantum gases, *Nature (London)* **494**, 49 (2013).
- [9] N. Goldman, G. Juzeliūnas, P. Öhberg, and I. B. Spielman, Light-induced gauge fields for ultracold atoms, *Rep. Prog. Phys.* **77**, 126401 (2014).
- [10] H. Zhai, Degenerate quantum gases with spin-orbit coupling: A review, *Rep. Prog. Phys.* **78**, 026001 (2015).
- [11] L. Huang, Z. Meng, P. Wang, P. Peng, S.-L. Zhang, L. Chen, D. Li, Q. Zhou, and J. Zhang, Experimental realization of two-dimensional synthetic spin-orbit coupling in ultracold Fermi gases, *Nat. Phys.* **12**, 540 (2016).
- [12] Z. Wu, L. Zhang, W. Sun, X.-T. Xu, B.-Z. Wang, S.-C. Ji, Y. Deng, S. Chen, X.-J. Liu, and J.-W. Pan, Realization of two-dimensional spin-orbit coupling for Bose-Einstein condensates, *Science* **354**, 83 (2016).
- [13] A. Celi, P. Massignan, J. Ruseckas, N. Goldman, I. B. Spielman, G. Juzeliūnas, and M. Lewenstein, Synthetic Gauge Fields in Synthetic Dimensions, *Phys. Rev. Lett.* **112**, 043001 (2014).
- [14] E. Anisimovas, M. Račiūnas, C. Sträter, A. Eckardt, I. B. Spielman, and G. Juzeliūnas, Semisynthetic zigzag optical lattice for ultracold bosons, *Phys. Rev. A* **94**, 063632 (2016).
- [15] M. Mancini, G. Pagano, G. Cappellini, L. Livi, M. Rider, J. Catani, C. Sias, P. Zoller, M. Inguscio, M. Dalmonte, and L. Fallani, Observation of chiral edge states with neutral fermions in synthetic Hall ribbons, *Science* **349**, 1510 (2015).
- [16] B. K. Stuhl, H.-I. Lu, L. M. Ayccock, D. Genkina, and I. B. Spielman, Visualizing edge states with an atomic Bose gas in the quantum Hall regime, *Science* **349**, 1514 (2015).
- [17] T. Ozawa and H. M. Price, Topological quantum matter in synthetic dimensions, *Nat. Rev. Phys.* **1**, 349 (2019).
- [18] O. Zilberberg, S. Huang, J. Guglielmon, M. Wang, K. P. Chen, Y. E. Kraus, and M. C. Rechtsman, Photonic topological boundary pumping as a probe of 4D quantum Hall physics, *Nature (London)* **553**, 59 (2018).

- [19] M. Lohse, C. Schweizer, H. M. Price, O. Zilberberg, and I. Bloch, Exploring 4D quantum Hall physics with a 2D topological charge pump, *Nature (London)* **553**, 55 (2018).
- [20] O. Boada, A. Celi, J. Rodríguez-Laguna, J. I. Latorre, and M. Lewenstein, Quantum simulation of non-trivial topology, *New J. Phys.* **17**, 045007 (2015).
- [21] J. H. Han, J. H. Kang, and Y. Shin, Band Gap Closing in a Synthetic Hall Tube of Neutral Fermions, *Phys. Rev. Lett.* **122**, 065303 (2019).
- [22] C.-H. Li, Y. Yan, S. Choudhury, D. B. Blasing, Q. Zhou, and Y. P. Chen, A Bose-Einstein condensate on a synthetic Hall cylinder, [arXiv:1809.02122](https://arxiv.org/abs/1809.02122).
- [23] R. P. Anderson, D. Trypogeorgos, A. Valdés-Curiel, Q.-Y. Liang, J. Tao, M. Zhao, T. Andrijauskas, G. Juzeliūnas, and I. B. Spielman, Realization of a deeply subwavelength adiabatic optical lattice, *Phys. Rev. Research* **2**, 013149 (2020).
- [24] X.-W. Luo, J. Zhang, and C. Zhang, Tunable flux through a synthetic Hall tube of neutral fermions, *Phys. Rev. A* **102**, 063327 (2020).
- [25] Y. Yan, S.-L. Zhang, S. Choudhury, and Q. Zhou, Emergent Periodic and Quasiperiodic Lattices on Surfaces of Synthetic Hall Tori and Synthetic Hall Cylinders, *Phys. Rev. Lett.* **123**, 260405 (2019).
- [26] S. Aubry and G. André, Analyticity breaking and Anderson localization in incommensurate lattices, *Ann. Isr. Phys. Soc.* **3**, 133 (1980).
- [27] R. B. Diener, G. A. Georgakis, J. Zhong, M. Raizen, and Q. Niu, Transition between extended and localized states in a one-dimensional incommensurate optical lattice, *Phys. Rev. A* **64**, 033416 (2001).
- [28] B. Damski, J. Zakrzewski, L. Santos, P. Zoller, and M. Lewenstein, Atomic Bose and Anderson Glasses in Optical Lattices, *Phys. Rev. Lett.* **91**, 080403 (2003).
- [29] J. Biddle, B. Wang, D. J. Priour, and S. Das Sarma, Localization in one-dimensional incommensurate lattices beyond the Aubry-André model, *Phys. Rev. A* **80**, 021603(R) (2009).
- [30] L. Fallani, J. E. Lye, V. Guarrera, C. Fort, and M. Inguscio, Ultracold Atoms in a Disordered Crystal of Light: Towards a Bose Glass, *Phys. Rev. Lett.* **98**, 130404 (2007).
- [31] G. Roati, C. D'Errico, L. Fallani, M. Fattori, C. Fort, M. Zaccanti, G. Modugno, M. Modugno, and M. Inguscio, Anderson localization of a non-interacting Bose-Einstein condensate, *Nature (London)* **453**, 895 (2008).
- [32] B. Kramer and A. MacKinnon, Localization: Theory and experiment, *Rep. Prog. Phys.* **56**, 1469 (1993).
- [33] See Supplemental Material at <http://link.aps.org/supplemental/10.1103/PhysRevLett.126.193001> for the interaction strength in cold atoms, which includes Refs. [34,35].
- [34] C. Chin, R. Grimm, P. Julienne, and E. Tiesinga, Feshbach resonances in ultracold gases, *Rev. Mod. Phys.* **82**, 1225 (2010).
- [35] M. Olshanii, Atomic Scattering in the Presence of an External Confinement and a Gas of Impenetrable Bosons, *Phys. Rev. Lett.* **81**, 938 (1998).
- [36] Q.-Y. Liang, D. Trypogeorgos, A. Valdés-Curiel, J. Tao, M. Zhao, and I. B. Spielman, Coherence and decoherence in the Harper-Hofstadter model, *Phys. Rev. Research* **3**, 023058 (2021).